

Article

The Activity and Cyclic Catalysis of Synthesized Iron-Supported Zr/Ti Solid Acid Catalysts in Methyl Benzoate Compounds

Chunjie Shi, Xiaofeng Yu ^{*}, Wei Wang, Haibing Wu, Ai Zhang and Shengjin Liu

School of Materials and Chemical Engineering, Bengbu University, Bengbu 233000, China

* Correspondence: yxf@bbc.edu.cn

Abstract: The catalytic activity and cyclic catalysis of different methyl benzoates were studied by using a series of Lewis solid acid catalysts. The iron-supported zirconium/titanium solid acid catalysts were characterized using FTIR, SEM, XRD, and BET. The details of catalytic activity and cyclic catalysis verified that the catalyst catalyzed the reactions of 31 benzoic acids with different substituents and methanol. In addition, the mechanism was revealed according to the microstructure, acid strength, and specific surface area of the catalysts, and the yields of methyl benzoates by the GC-MS. Zr ions had significant effects on the catalytic activity of the catalyst. A certain proportion of Fe and Ti ions additionally enhanced the catalytic activity of the catalyst, with the catalyst-specific composition of Fe:Zr:Ti = 2:1:1 showing optimal catalytic activity. A variety of substituents in the benzene ring, such as the electron-withdrawing group, the electron-donating group, large steric hindrance, and the position of the group on the benzene ring, had regular effects on the catalytic activity of the methyl benzoates. An increase in the catalyst activity occurred owing to the increases in the catalyst surface and the number of acid sites after the Fe ion was added. The catalytic activity remained unchanged after the facile recycling method was performed.

Keywords: zirconium/titanium solid acid; iron-supported; methyl benzoate compounds



Citation: Shi, C.; Yu, X.; Wang, W.; Wu, H.; Zhang, A.; Liu, S. The Activity and Cyclic Catalysis of Synthesized Iron-Supported Zr/Ti Solid Acid Catalysts in Methyl Benzoate Compounds. *Catalysts* **2023**, *13*, 971. <https://doi.org/10.3390/catal13060971>

Academic Editors:
Katabathini Narasimharao and
Maqsood Ahmad Malik

Received: 11 May 2023
Revised: 28 May 2023
Accepted: 29 May 2023
Published: 2 June 2023



Copyright: © 2023 by the authors. Licensee MDPI, Basel, Switzerland. This article is an open access article distributed under the terms and conditions of the Creative Commons Attribution (CC BY) license (<https://creativecommons.org/licenses/by/4.0/>).

1. Introduction

Methyl benzoates are intermediate compounds in the chemical industry that are directly used as spices, additives in daily chemical products, and preservatives [1–3]. Two types of catalysts are used for the synthesis of methyl benzoate compounds: homogeneous and heterogeneous. Classical catalysts primarily involve sulfuric, phosphoric, and *p*-toluene sulfonic acids, which have poor selectivity, produce oxidized byproducts, are difficult to recycle, and cause waste-acid pollution [4–8]. Therefore, there is an urgent need to develop environmentally friendly and economical catalysts for the preparation of methyl benzoates. Heterogeneous catalysts for the synthesis of methyl benzoate compounds have been extensively reported, including heteropoly acid catalysts, strong acid cationic resins, molecular sieves, and solid superacids [9,10]. In recent years, solid acid catalysts have replaced chemical acid catalysts because of their convenience, nontoxicity, non-corrosiveness, environmental protection, low price, easy mass production, and easy recycling [11–14]. This has attracted attention as an attractive topic for the catalytic synthesis of methyl benzoate.

Solid acid [11,15,16] catalysts were silica–aluminum gels used to crack hydrocarbons in the early chemical industry. Further series of catalysts, such as $\text{SO}_4^{2-}/\text{M}_x\text{O}_y$ solid acid catalysts, have shown obvious advantages for ester synthesis. However, in a previous study, these catalysts exhibited sensitivity to water or were unstable after sulfate leaching [17–19]. The number of active sites and specific surface area of a solid catalyst directly affect its catalytic activity. The combination of catalytic activity and cycling stability is a significant challenge in the design and fabrication of solid acid catalysts.

Titanium and zirconium phosphate catalysts are widely used in organic synthesis. However, most of them are individual Ti or Zr catalysts, and there are few reports on composite catalysts. The ternary phase catalyst used to synthesize methyl benzoates has not been reported on. There are few reports on the catalytic efficiency of three-way catalytic materials.

Although solid acid catalysts have been widely used in various ester syntheses and photocatalyses, mounts of solid acid catalysts still need carrier materials, such as carbon or inorganic porous materials [1,20]. Moreover, the preparation and catalytic activity of the catalyst is considered based on the specific surface area of the carrier and chemical activity. Significant restrictions in recycling catalysts are the complex recovery processes and the reduction in catalytic activity.

The current study aims to synthesize a series of solid acid catalysts in which the catalytic activity and selectivity of the catalysts are revealed for the synthesis of methyl benzoate compounds. A carrier-free solid acid catalyst was developed, which still maintained high catalytic efficiency in facile recycling.

2. Results and Discussion

2.1. Characteristics of the Catalyst

The synthesized catalysts which have different contains of Ti, Fe, and Zr (as listed in Table 1) were characterized using XRD, FT-IR, and SEM. The XRD results showed a weak diffraction intensity for all the catalysts owing to the large amount of amorphous phase in the catalyst, as shown in Figure 1. $\text{Fe}_2(\text{SO}_4)_3$, $\text{Ti}_2(\text{SO}_4)_3$, $\text{Ti}(\text{SO}_4)_2$, and $\text{Zr}(\text{SO}_4)_2$ were then separated. However, amorphous phases, such as $\text{Fe}_2(\text{SO}_4)_3$, $\text{Ti}_2(\text{SO}_4)_3$, $\text{Ti}(\text{SO}_4)_2$, and $\text{Zr}(\text{SO}_4)_2$, were the primary phases in the catalytic process. Compared with all the catalyst curves, only small amounts of the crystal phases of $\text{Fe}_2(\text{SO}_4)_3$, $\text{Ti}_2(\text{SO}_4)_3$, $\text{Ti}(\text{SO}_4)_2$, and $\text{Zr}(\text{SO}_4)_2$ are shown in ZFT01, ZFT04, ZF07, and ZT08 (Table 1), respectively. This implies that the amorphous phase of the sulfate was primary in the catalyst. The ordered microstructure of S_8 is shown in the ZFT05 (Table 1) catalyst, which has a high peak in $2\theta = 23.005$. A plausible explanation is that the tetrahedron $(\text{SO}_4)^{2-}$ exhibited the ordered arrangement.

Table 1. The effect of iron/zirconium/titanium catalyst type on the esterification of *p*-methylbenzoate and methyl *p*-chlorobenzoate ^a.

	Zirconium Oxochloride: Ferric Chloride Hexahydrate: Tetrabutyl Titanate (Molar Ratio)	Yield of Methyl <i>p</i> -Methylbenzoate (%)	Yield of Methyl <i>p</i> -Chlorobenzoate (%) ^b
ZFT01	1:1:1	49.0	45.3
ZFT02	1:1:0.5	25.1	22.1
ZFT03	1:1:2	23.6	20.2
ZFT04	1:2:1	60.9	57.2
ZFT05	1:0.5:1	45.8	40.3
FT06	0:1:1	19.6	17.3
ZF07	1:1:0	56.0	52.8
ZT08	1:0:1	50.4	50.4

^a Reaction conditions: acid (0.5 g), CH_3OH (10 mL), cat. (0.05 g), oil bath (120 °C), 6 h. ^b Isolated yields.

A small amount of the oxide products is shown in ZFT04, ZFT05, and FT06 (Figure 1). The diffraction peaks of the oxides and Rosickyite (S_8 , PDF:53-1109) appear in ZFT03, ZFT04, ZFT05, FT06, and ZF07. Maghemite-Q (Fe_2O_3 , PDF: 25-1402) showed weak peaks in all curves except ZT08. The diffraction intensity gradually increased with the increase in iron content. That is, excessive iron in the catalyst was converted into Fe_2O_3 rather than iron sulfate. The weak peaks of titanium oxide (TiO_2 , PDF:46-1238) and zirconium oxide (ZrO_2 , PDF:42-1164) revealed that a higher temperature was perhaps needed to form ZrO_2 and TiO_2 .

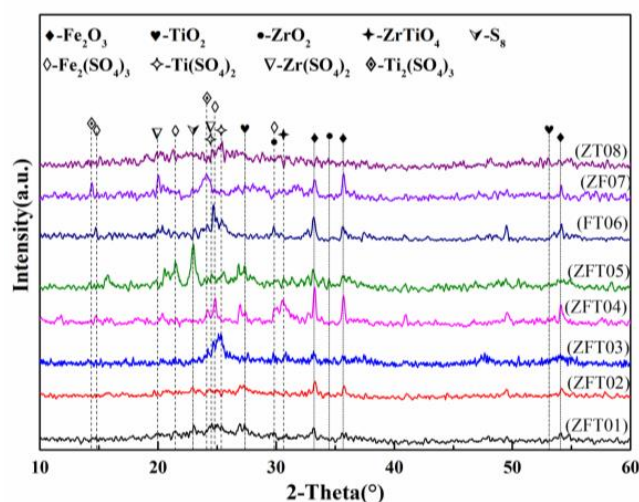


Figure 1. XRD curves of the catalysts.

The iron addition promoted crystal formation in the heating process, which increased the split phase and increased the number of acidic sites, namely the active center. The surface area increased due to the grains growing out of the catalyst's matrix. It is an important cause that the addition of iron increases the catalytic activity of the catalyst.

The FT-IR showed the main bond in the catalysts (Figure 2). The infrared multiple absorption peak at $1040\text{--}1180\text{ cm}^{-1}$ (Figure 2) was attributed to the S=O double bond. It was revealed that the $[\text{SO}_4]$ was bonded to the catalyst. The peak at 1400 cm^{-1} was attributed to the vibrational absorption of the covalent S=O double bond, which is the characteristic absorption of a solid superacid. This finding indicates the successful synthesis of the solid superacid. The other absorption peaks belonging to the solid catalysts are not detailed.

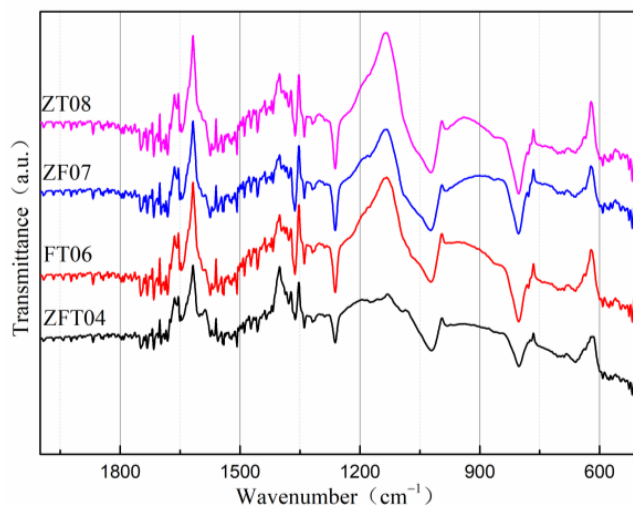


Figure 2. FT-IT curves of the catalysts.

SEM images clearly showed a porous structural microstructure in all the catalysts, as shown in Figure 3. The size of the near-spherical pores in ZFT06 was in the range of 300–600 nm (Figure 3a,b). The uniformity of the micron-size pores is shown in ZT06 (Figure 3c,d). That is, Fe addition has a great influence on the pore structure of the synthesized catalyst. The addition of the Fe ion reduced the size of the pore structure and further regulated the pore to be spherical through surface tension, which increased the specific surface area of the catalyst and improved the catalytic activity of the catalyst. It improved the contact area between the catalyst and the raws, and increased the catalytic activity.

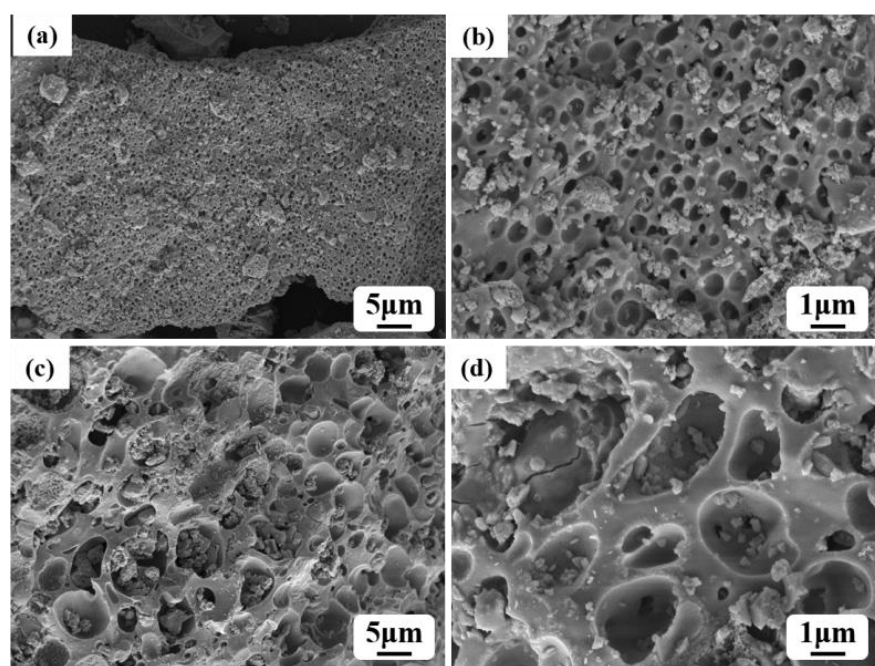


Figure 3. SEM images of the catalysts. (a–d) are microstructure images of FT06 and ZFT04, respectively.

In addition, a small number of the nanograins, which are the active catalytic particles formed in the heating process of the catalyst synthesis via in situ growth, were dispersed in the amorphous matrix and pores. These nanograins had a regular edge and their size was in the range of 100–300 nm. The grains increased the specific surface area of the catalyst and provided more catalytic active sites for the catalytic reaction.

2.2. Catalyst Activity in Esterification

The synthesis of methyl benzoate was catalyzed by a series of synthesized iron/zirconium/titanium catalysts. The activities of the catalysts were determined by the product yield after 6 h. The yields of methyl *p*-methylbenzoate and methyl *p*-chlorobenzoate are listed in Table 1.

Both methyl *p*-methylbenzoate and methyl *p*-chlorobenzoate showed optimal yields upon adding catalyst ZFT04, which had Zr and the highest ferric ratio. Zr has primary catalytic effects in the catalytic process, as shown in the comparison of the yields of FT06, ZF07, and ZT08. Lower or higher titanium additions can inhibit the catalytic effects. An increase in the iron content can promote the catalytic effects of the catalyst, owing to the firmness of the sulfate. Based on the XRD results, the iron in the catalyst assisted in the formation of a catalytically active center through combination with the sulfate, further enhancing the catalytic effects. The precipitation of the fine grains produced active reaction sites, which promoted the catalytic reaction.

2.3. Reaction of Benzoic Acid Derivatives

A series of catalytic activities of different esters were studied using the preferred catalyst ZFT04. In addition, the catalytic mechanism of the catalyst was revealed. The groups in the benzene ring that affected the ester yield were identified by the esterification reactions of different starting materials. The results are shown in Table 2. The yields were in the following order: 93.5% (*p*-CH₃) > 85.1% (*m*-CH₃) > 82.3% (*o*-CH₃), 90.0% (*p*-Cl) > 84.3% (*m*-Cl) > 82.2% (*o*-Cl), 80.4% (*p*-Br) > 77.8% (*m*-Br) > 63.5% (*o*-Br), 85.1% (*p*-Br) > 83.0% (*m*-Br) > 80.1% (*o*-Br), and 97.5% (*p*-Br) > 92.1% (*m*-Br) > 87.7% (*o*-Br). The steric effect was found to exert a stronger effect in catalytic reactions in which the materials have ortho-para substituents on the benzene ring. The substituents at the proximal position exhibited the lowest catalytic activity. With an electron-withdrawing group in the meta-position of

the benzene ring, the catalyst had weak catalytic activity due to the electronic effect; the yields were in the following order: 65.3% (*p*-CF₃) > 45.3% (*o*-CF₃) > 35.2% (*m*-CF₃), 70.8% (*p*-NO₂) > 65.3% (*o*-NO₂) > 50.1% (*m*-NO₂), and 90.8% (*p*-OCH₃) > 85.1% (*o*-OCH₃) > 80.2% (*m*-OCH₃). Benzoic acid, which has double carboxyl groups, showed lower reactivity upon catalyst addition due to the strong electron-withdrawing group of carboxylic acid and strong steric hindrance. The para-position groups in the benzene ring had little effect on the catalytic activity, even if they exhibited a large steric hindrance, as shown by the yields: 88.7% (*t*-Bu) and 86.8% (CN). The catalyst exhibited decent activity, regardless of whether the benzene ring had an electron-withdrawing or electron-donating group.

Table 2. Synthesis of methyl benzoate derivatives by epidicatalysis.

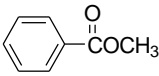
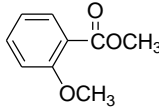
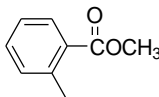
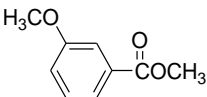
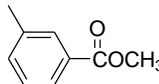
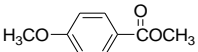
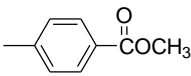
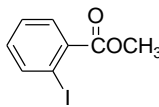
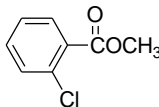
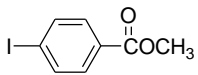
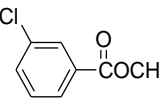
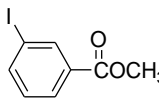
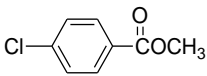
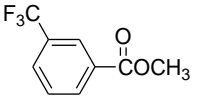
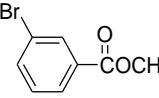
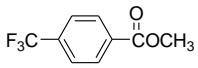
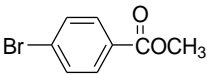
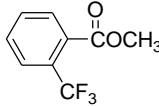
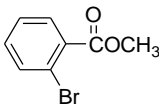
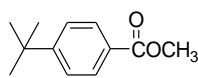
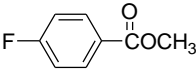
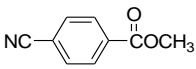
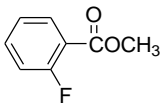
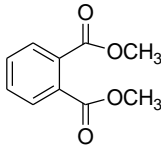
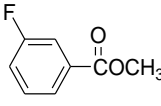
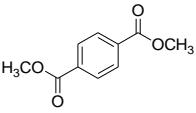
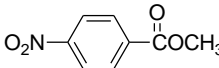
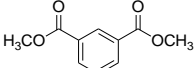
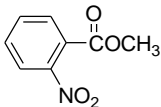
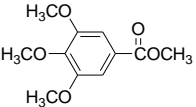
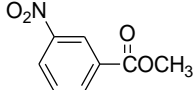
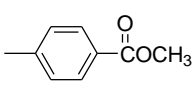
Entry	Ester	Time (h)	Yield (%) ^a	Entry	Ester	Time (h)	Yield (%) ^a
1		24	90.2	17		24	85.1
2		24	82.3	18		24	80.2
3		24	85.1	19		24	90.8
4		24	93.5	20		24	80.1
5		24	82.2	21		24	85.2
6		24	84.3	22		24	83.0
7		24	90.0	23		24	35.2
8		24	77.8	24		24	65.3
9		24	80.4	25		24	45.3
10		24	63.5	26		24	88.7

Table 2. Cont.

Entry	Ester	Time (h)	Yield (%) ^a	Entry	Ester	Time (h)	Yield (%) ^a
11		24	97.5	27		24	86.8
12		24	87.8	28		24	53.5
13		24	92.1	29		24	60.2
14		24 48	45.2 70.8	30		24	56.1
15		24 48	35.2 65.3	31		24	68.7
16		24 48	34.3 50.1	32 ^b		24	92.8

^a Isolated yields; ^b recovered catalyst.

Because the esterification reaction is heterogeneous, the catalyst and reactants can be directly separated by solid–liquid separation after the initial reaction. After the reaction liquid was filtered and discarded, new reactants were added. The activity of the second reaction was similar to that of the first. The activity of the secondary recycled catalyst was almost unchanged. Typically, the yields were 93.5% (entry 4) and 92.8% (entry 32) with the use of the recycled catalyst, and the fifth recycled catalyst showed high stable catalytic activity, with the yields having decreased to 93.0% and 92.0%, respectively.

The reactions and mechanism of the 31 benzoic acids with different substituents and methanol are shown in Figure 4. According to the Thomas law, the addition of iron ions has a lower valence state than zirconium and titanium ions, which form acidic centers with zirconium and titanium, respectively, in the system, improving catalytic activity. The Lewis acid sites easily formed π bond complexes with aromatics. The acid strength of the synthesized catalyst was lower than -11.93 , which caused the hydrogenation of the bond complex. That is, the acid sites provided by the hydrogen ion activated the carbonyl group, which promoted the esterification reaction.

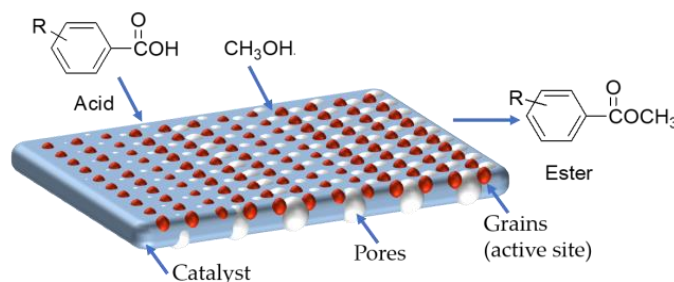


Figure 4. The reactions and mechanism of methyl benzoate derivatives.

2.4. Properties and Activity of the Preferred Catalyst

The acid strengths of ZFT04 were determined using a Hammett indicator (H_0). The solid superacid could significantly change the color of 2,4-dinitrotoluene ($H_0 = -13.75$) and 2,4-dinitrofluorobenzene ($H_0 = -14.52$), but that of 1,3,5-trinitrobenzene ($H_0 = -16.02$) did not change. This catalyst was a superacid and the acid strength range was $-16.02 < H_0 < -14.52$. This indicated that the solid acid was a solid superacid.

The pore structures of ZFT04 were analyzed using N_2 adsorption/desorption tests (Figure 5). The type IV H1 hysteresis loop of IUPAC classification was shown in the ZFT04 and regenerated ZFT04 N_2 adsorption/desorption curves. The adsorption amount increased gently in the low-pressure section, and N_2 molecules were adsorbed on the inner surface of the mesoporous material from a single layer to multiple layers. When $P/P_0 = 0.5-0.8$, the adsorption capacity increased sharply. This section revealed that the pore size of the sample showed ion accumulation, with an ordered or gradient mesoporous range in the pore structure. In addition, its width was relatively narrow, indicating that the pore size distribution was uniform.

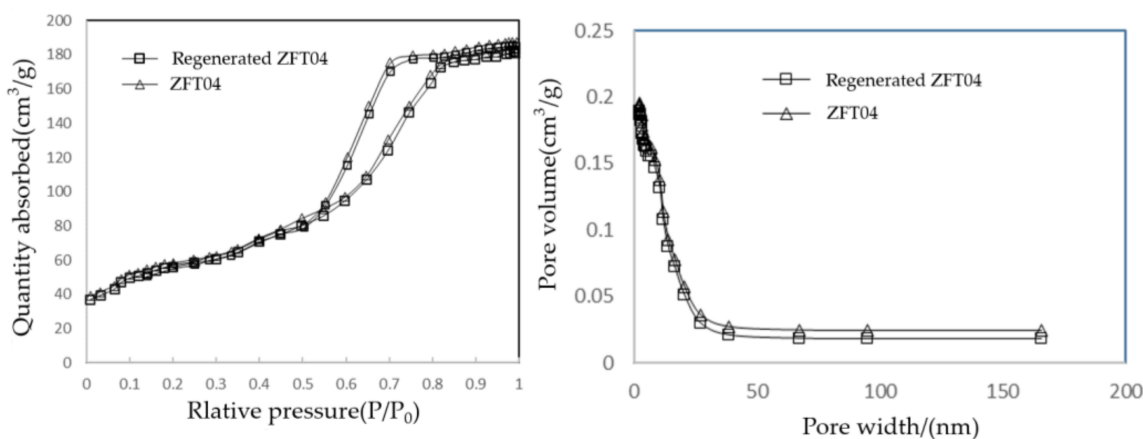


Figure 5. The N_2 adsorption/desorption isotherms and pore size distribution of ZFT04 and generated ZFT04.

The surface area of the catalyst was $322 \text{ cm}^2/\text{g}$ (Table 3), which was larger than those of the reported porous Fe_2O_3 , TiO_2 , and ZrO_2 . This indicates that the synthesis of the catalyst did not destroy the pore structure and retained the original pore structure of the carrier. The N_2 adsorption/desorption curves showed that the recovered catalyst had the same pore structure and specific surface area as the original catalyst (Figure 5).

Table 3. Surface properties of the different ZFT04 samples.

Samples	Surface Area (cm^2/g)	s	Pore Diameter (nm)
ZFT04	322	0.246	2.75
Regenerated ZFT04	318	0.244	2.74

These newly synthesized solid acid catalysts have comparable activity in the synthesis of benzoate compared with the use of sulfuric acid. The catalytic reaction is heterogeneous and the catalyst can simply be recycled and reused. In industry, these solid acids can completely replace sulfuric acid. The next research plan of our research group is to fill solid acid catalysts in the column. The liquid reaction is carried out in a continuous flow reaction in the column.

3. Materials and Methods

3.1. Synthesis of Solid Acid Catalysts

Dichlorooxozirconium, iron (III) chloride hexahydrate, tetrabutyl titanate, and methanol were purchased from Sinopharm Chemical Reagent Co. Ltd., Shanghai, China. Benzoic acid and other benzene compounds were purchased from Aladdin Reagent Co. Ltd., Shanghai, China. Deionized water (18.2 M Ω ·cm) was used in the catalyst synthesis. All materials were used as received.

A 50% dichlorooxozirconium solution and 30% iron (III) chloride were prepared and mixed after weighing according to the molar ratios listed in Table 1. Tetrabutyl titanate was added to the mixture solution under rapid stirring. Thereafter, the mixture was put in the oven at 100 °C and held for more than 12 h, until a constant weight was attained. Next, the dry powder was dipped in sulfuric acid (2 mol/L) for 24 h and was put into the oven at 120 °C for 24 h to dry. Finally, the dried powder was put into a Muffle furnace and heated at 550 °C for 12 h.

3.2. General Catalytic Process

Total amounts of 0.50 g benzoic acid, 10.00 mL methanol, and 0.05 g catalyst ZFT04 were placed in flasks. The mixture was stirred in an oil bath at 120 °C, and the progress of the reaction was monitored using TLC. In an oil bath at 120 °C, the mixture was strongly refluxed. If there was too little methanol during reflux, a small amount could be added. After the predetermined reflux time, the catalyst was filtered out from the liquid phase, the methanol was spin-dried, and the product was dissolved in ethyl acetate. The mobile phase was petroleum ether: ethyl acetate (5:1).

3.3. Recovery Catalyst Catalytic Process

After the catalyst was recovered, it was baked at 100 °C until a constant weight was reached. The catalysis procedure was the same as that for a general catalytic process.

3.4. Characterization of Methyl Benzoates

Methyl benzoate (1) [21]: Clear liquid; ¹H NMR (400 MHz, CDCl₃): δ = 8.01 (d, J = 8.0 Hz, 2H), 7.50 (t, J = 8.0 Hz, 1H), 7.48 (t, J = 8.0 Hz, 2H), 3.84 (s, 3H); ¹³C NMR (100 MHz, CDCl₃): δ = 166.69, 132.71, 130.11, 129.42, 128.20, 51.73; HRMS (ESI-TOF) m/z : calcd for C₈H₇INaO²⁺: 159.0419 (M + Na)⁺, found: 159.0417 (Figure S1: ¹H and ¹³C NMR of Methyl benzoate).

Methyl 2-methylbenzoate (2) [21]: Yellow liquid; ¹H NMR (400 MHz, CDCl₃): δ = 7.82 – 7.80 (m, 2H), 7.28 – 7.22 (m, 2H), 3.82 (s, 3H), 2.31 (m, 3H); ¹³C NMR (100 MHz, CDCl₃): δ = 166.80, 137.86, 133.43, 130.01, 129.94, 128.06, 126.56, 51.61, 20.91; HRMS (ESI-TOF) m/z : calcd for C₉H₁₀NaO²⁺: 172.1745 (M + Na)⁺, found: 172.1811 (Figure S2: ¹H and ¹³C NMR of Methyl 2-methylbenzoate).

Methyl 3-methylbenzoate (3) [21]: Clear liquid; ¹H NMR (400 MHz, CDCl₃): δ = 7.88 (dd, J = 8.2, 1.6 Hz, 1H), 7.33 (td, J = 8.2, 1.6 Hz, 1H), 7.29 – 7.18 (m, 2H), 3.81 (s, 3H), 2.57 (s, 3H); ¹³C NMR (100 MHz, CDCl₃): δ = 167.69, 140.12, 131.84, 131.59, 130.54, 129.45, 125.59, 51.49, 21.59; HRMS (ESI-TOF) m/z : calcd for C₉H₁₀NaO²⁺: 172.1745 (M + Na)⁺, found: 172.1521 (Figure S3; ¹H and ¹³C NMR of Methyl 3-methylbenzoate).

Methyl 4-methylbenzoate (4) [21,22]: White solid; mp 33–35 °C; ¹H NMR (400 MHz, CDCl₃): δ = 7.92 (d, J = 8.0 Hz, 2H), 7.20 (d, J = 8.0 Hz, 2H), 3.87 (s, 3H), 2.37 (s, 3H); ¹³C NMR (100 MHz, CDCl₃): δ = 167.04, 143.46, 129.56, 129.02, 127.43, 51.80, 21.52; HRMS (ESI-TOF) m/z : 150.1745 calcd for C₉H₁₀NaO²⁺: 172.1745 (M + Na)⁺, found: 172.1701 (Figure S4; ¹H and ¹³C NMR of Methyl 4-methylbenzoate).

Methyl 2-chlorobenzoate (5) [23]: Clear liquid; ¹H NMR (400 MHz, CDCl₃): δ = 7.80 (dd, J = 8.0, 1.0 Hz, 1H), 7.48 – 7.39 (m, 2H), 7.35 (td, J = 8.0 Hz, 1.2 Hz, 1H), 3.90 (s, 3H); ¹³C NMR (100 MHz, CDCl₃): δ = 165.85, 133.46, 132.48, 131.29, 130.90, 129.92, 126.51, 52.21; HRMS (ESI-TOF) m/z : calcd for C₈H₇ClNaO²⁺: 193.0028 (M + Na)⁺, found: 193.0027 (Figure S5; ¹H and ¹³C NMR of Methyl 2-chlorobenzoate).

Methyl 3-chlorobenzoate (**6**) [21,23]: Clear liquid; ^1H NMR (400 MHz, CDCl_3): $\delta = 7.98$ (m, 1H), 7.88 (m, 1H), 7.49 (m, 1H), 7.36 (t, $J = 8.0$ Hz, 1H), 3.90 (s, 3H); ^{13}C NMR (100 MHz, CDCl_3): $\delta = 168.17, 134.39, 132.80, 131.79, 129.60, 129.52, 127.60, 52.05$; HRMS (ESI-TOF) m/z : calcd for $\text{C}_8\text{H}_7\text{ClNaO}^{2+}$: 193.0026 ($\text{M} + \text{Na}$) $^+$, found: 193.0015 (Figure S6: ^1H and ^{13}C NMR of Methyl 3-chlorobenzoate).

Methyl 4-chlorobenzoate (**7**) [21,23]: Clear liquid; ^1H NMR (400 MHz, CDCl_3): $\delta = 7.92$ (d, $J = 8.0$ Hz, 2H), 7.20 (d, $J = 8.0$ Hz, 2H), 3.87 (s, 3H); ^{13}C NMR (100 MHz, CDCl_3): $\delta = 167.04, 143.46, 129.56, 129.02, 127.44, 51.80$; HRMS (ESI-TOF) m/z : calcd for $\text{C}_8\text{H}_7\text{ClNaO}^{2+}$: 193.0026 ($\text{M} + \text{Na}$) $^+$, found: 193.0019 (Figure S7: ^1H and ^{13}C NMR of Methyl 4-chlorobenzoate).

Methyl 3-bromobenzoate (**8**) [21,23]: White solid; mp 31–33 °C; ^1H NMR (400 MHz, CDCl_3): $\delta = 8.15$ (m, 1H), 7.92 (m, 1H), 7.64 (m, 1H), 7.29 (t, $J = 8.0$ Hz, 1H), 3.90 (s, 3H); ^{13}C NMR (100 MHz, CDCl_3): $\delta = 165.52, 135.75, 132.48, 131.99, 129.88, 128.07, 122.38, 52.31$; HRMS (ESI-TOF) m/z : calcd for $\text{C}_8\text{H}_7\text{BrNaO}^{2+}$: 236.9526 ($\text{M} + \text{Na}$) $^+$, found: 236.9517 (Figure S8: ^1H and ^{13}C NMR of Methyl 3-bromobenzoate).

Methyl 4-bromobenzoate (**9**) [21,23]: White solid; mp 77–80 °C; ^1H NMR (400 MHz, CDCl_3): $\delta = 7.88$ (m, 2H), 7.56 (m, 2H), 3.90 (s, 3H); ^{13}C NMR (100 MHz, CDCl_3): $\delta = 166.23, 131.66, 131.08, 129.01, 127.99, 52.24$; HRMS (ESI-TOF) m/z : calcd for $\text{C}_8\text{H}_7\text{BrNaO}^{2+}$: 236.9526 ($\text{M} + \text{Na}$) $^+$, found: 236.9515 (Figure S9: ^1H and ^{13}C NMR of Methyl 4-bromobenzoate).

Methyl 2-bromobenzoate (**10**) [23]: Clear liquid; ^1H NMR (400 MHz, CDCl_3): $\delta = 7.78$ (dd, $J = 7.8, 1.0$ Hz, 1H), 7.63 (dd, $J = 7.5, 1.0$ Hz, 1H), 7.33 – 7.27 (m, 2H), 3.91 (s, 3H); ^{13}C NMR (100 MHz, CDCl_3): $\delta = 166.44, 134.25, 132.55, 132.06, 131.25, 127.14, 121.55, 52.39$; HRMS (ESI-TOF) m/z : calcd for $\text{C}_8\text{H}_7\text{BrNaO}^{2+}$: 236.9526 ($\text{M} + \text{Na}$) $^+$, found: 236.9514 (Figure S10: ^1H and ^{13}C NMR of Methyl 2-bromobenzoate).

Methyl 4-fluorobenzoate (**11**) [21,23]: Clear liquid; ^1H NMR (400 MHz, CDCl_3): $\delta = 8.03$ (dd, $J = 8.4, 5.6$ Hz, 2H), 7.08 (t, $J = 8.5$ Hz, 2H), 3.89 (s, 3H); ^{13}C NMR (100 MHz, CDCl_3): $\delta = 166.84, 165.76$ (d, $J_{\text{C-F}} = 253$ Hz), 131.98 (d, $J_{\text{C-F}} = 9.0$ Hz), 115.36 (d, $J_{\text{C-F}} = 3.0$ Hz), 115.14 (d, $J_{\text{C-F}} = 21.9$ Hz), 51.82; ^{19}F NMR (376 MHz, CDCl_3): $\delta = 106.14$; HRMS (ESI-TOF) m/z : calcd for $\text{C}_8\text{H}_7\text{FNaO}^{2+}$: 177.0325 ($\text{M} + \text{Na}$) $^+$, found: 177.0320 (Figure S11: ^1H , ^{13}C and ^{19}F NMR of Methyl 4-fluorobenzoate).

Methyl 2-fluorobenzoate (**12**) [21,23]: Clear liquid; ^1H NMR (400 MHz, CDCl_3): $\delta = 7.92$ (td, $J = 7.9, 1.64$ Hz, 1H), 7.47 (m, 1H), 7.19 (t, $J = 8.2$ Hz, 1H), 7.12 (dd, $J = 10.5, 9.0$ Hz, 1H), 3.92 (s, 3H); ^{13}C NMR (100 MHz, CDCl_3): $\delta = 164.74$ (d, $J_{\text{C-F}} = 3.8$ Hz), 160.54 (d, $J_{\text{C-F}} = 260$ Hz), 134.47 (d, $J_{\text{C-F}} = 9.2$ Hz), 132.04, 123.86 (d, $J_{\text{C-F}} = 4.0$ Hz), 118.60 (d, $J_{\text{C-F}} = 10$ Hz), 116.97 (d, $J_{\text{C-F}} = 22.3$ Hz), 52.13; ^{19}F NMR (376 MHz, CDCl_3): $\delta = 109.68$; HRMS (ESI-TOF) m/z : calcd for $\text{C}_8\text{H}_7\text{FNaO}^{2+}$: 177.0321 ($\text{M} + \text{Na}$) $^+$, found: 177.0324 (Figure S12: ^1H , ^{13}C and ^{19}F NMR of Methyl 2-fluorobenzoate).

Methyl 3-fluorobenzoate (**13**) [23]: Clear liquid; ^1H NMR (400 MHz, CDCl_3): $\delta = 7.69$ (d, $J = 7.7$ Hz, 1H), 7.39 (d, $J = 9.3$ Hz, 1H), 7.25 – 7.23 (m, 1H), 7.22 (m, 1H), 3.91 (s, 3H); ^{13}C NMR (100 MHz, CDCl_3): $\delta = 165.81$ (d, $J_{\text{C-F}} = 3.2$ Hz), 163.67 (d, $J_{\text{C-F}} = 245.0$ Hz), 132.25 (d, $J_{\text{C-F}} = 7.2$ Hz), 129.96 (d, $J_{\text{C-F}} = 7.5$ Hz), 125.23 (d, $J_{\text{C-F}} = 3.0$ Hz), 119.72 (d, $J_{\text{C-F}} = 21$ Hz), 116.40 (d, $J_{\text{C-F}} = 25$ Hz), 52.41; ^{19}F NMR (376 MHz, CDCl_3): $\delta = 112.56$; HRMS (ESI-TOF) m/z : calcd for $\text{C}_8\text{H}_7\text{FNaO}^{2+}$: 177.0324 ($\text{M} + \text{Na}$) $^+$, found: 177.0317 (Figure S13: ^1H , ^{13}C and ^{19}F NMR of Methyl 3-fluorobenzoate).

Methyl 4-nitrobenzoate (**14**) [22,23]: Yellow solid; mp 94–97 °C; ^1H NMR (400 MHz, CDCl_3): $\delta = 8.29$ (d, $J = 8.0$ Hz, 2H), 8.21 (d, $J = 8.5$ Hz, 2H), 3.99 (s, 3H); ^{13}C NMR (100 MHz, CDCl_3): $\delta = 165.11, 150.48, 135.45, 130.66, 123.49, 52.79$; HRMS (ESI-TOF) m/z : calcd for $\text{C}_8\text{H}_7\text{NNaO}^{4+}$: 204.0277 ($\text{M} + \text{Na}$) $^+$, found: 204.0267 (Figure S14: ^1H and ^{13}C NMR of Methyl 4-nitrobenzoate).

Methyl 2-nitrobenzoate (**15**) [22,23]: Yellow liquid; ^1H NMR (400 MHz, CDCl_3): $\delta = 7.88$ (dd, $J = 7.8, 0.9$ Hz, 1H), 7.70 – 7.62 (m, 3H), 3.91 (s, 3H); ^{13}C NMR (100 MHz, CDCl_3): $\delta = 165.52, 148.09, 132.94, 131.96, 129.70, 126.97, 123.71, 52.91$; HRMS (ESI-TOF) m/z : calcd for $\text{C}_8\text{H}_7\text{NNaO}^{4+}$: 204.0268 ($\text{M} + \text{Na}$) $^+$, found: 204.0271 (Figure S15: ^1H and ^{13}C NMR of Methyl 2-nitrobenzoate).

Methyl 3-nitrobenzoate (**16**) [22,23]: Yellow solid; mp 76–80 °C; ^1H NMR (400 MHz, CDCl_3): δ = 8.86 (s, 1H), 8.42 (dd, J = 8.0, 1.0 Hz, 1H), 8.37 (d, J = 8.0 Hz, 1H), 7.68 (t, J = 8.0 Hz, 1H), 4.00 (s, 3H); ^{13}C NMR (100 MHz, CDCl_3): δ = 164.88, 148.20, 135.22, 131.81, 129.66, 127.33, 124.47, 52.75; HRMS (ESI-TOF) m/z : calcd for $\text{C}_8\text{H}_7\text{NNaO}^{4+}$: 204.0269 ($\text{M} + \text{Na}$) $^+$, found: 204.0257 (Figure S16: ^1H and ^{13}C NMR of Methyl 3-nitrobenzoate).

Methyl 2-methoxybenzoate (**17**) [23]: Clear liquid; ^1H NMR (400 MHz, CDCl_3): δ = 7.76 (dd, J = 8.0, 1.6 Hz, 1H), 7.39 (td, J = 8.2, 1.3 Hz, 1H), 6.94 – 6.90 (m, 2H), 3.82 (s, 6H); ^{13}C NMR (100 MHz, CDCl_3): δ = 166.25, 158.75, 133.18, 131.19, 119.92, 119.76, 111.79, 55.41, 51.43; HRMS (ESI-TOF) m/z : calcd for $\text{C}_9\text{H}_{10}\text{NaO}^{3+}$: 189.0524 ($\text{M} + \text{Na}$) $^+$, found: 189.0527 (Figure S17: ^1H and ^{13}C NMR of Methyl 2-methoxybenzoate).

Methyl 3-methoxybenzoate (**18**) [21,23]: Clear liquid; ^1H NMR (400 MHz, CDCl_3): δ = 7.60 (d, J = 7.9 Hz, 1H), 7.53 (s, 1H), 7.28 (t, J = 8.2 Hz, 1H), 7.04 (dd, J = 7.6, 1.9 Hz, 1H), 3.86 (s, 3H), 3.76 (s, 3H); ^{13}C NMR (100 MHz, CDCl_3): δ = 166.52, 159.43, 131.31, 129.16, 121.68, 119.00, 113.93, 54.95, 51.74; HRMS (ESI-TOF) m/z : calcd for $\text{C}_9\text{H}_{10}\text{NaO}^{3+}$: 189.0524 ($\text{M} + \text{Na}$) $^+$, found: 189.0521 (Figure S18: ^1H and ^{13}C NMR of Methyl 3-methoxybenzoate).

Methyl 4-methoxybenzoate (**19**) [21–23]: White solid; mp 47–51 °C; ^1H NMR (400 MHz, CDCl_3): δ = 8.0 (d, J = 8.2 Hz, 2H), 6.89 (d, J = 8.2 Hz, 2H), 3.85 (s, 3H), 3.81 (s, 3H); ^{13}C NMR (100 MHz, CDCl_3): δ = 166.75, 163.3, 131.52, 122.54, 113.55, 55.30, 51.74; HRMS (ESI-TOF) m/z : calcd for $\text{C}_9\text{H}_{10}\text{NaO}^{3+}$: 189.0525 ($\text{M} + \text{Na}$) $^+$, found: 189.0521 (Figure S19: ^1H and ^{13}C NMR of Methyl 4-methoxybenzoate).

Methyl 2-iodobenzoate (**20**) [23]: Yellow liquid; ^1H NMR (400 MHz, CDCl_3): δ = 7.96 (d, J = 8.0 Hz, 1H), 7.77 (dd, J = 8.0, 1.0 Hz, 1H), 7.34 (t, J = 7.6 Hz, 1H), 7.12 (td, J = 7.8, 1.5 Hz, 1H), 3.90 (s, 3H); ^{13}C NMR (100 MHz, CDCl_3): δ = 166.73, 141.23, 134.97, 132.68, 130.92, 127.92, 94.16, 52.50; HRMS (ESI-TOF) m/z : calcd for $\text{C}_8\text{H}_7\text{INaO}^{2+}$: 284.9385 ($\text{M} + \text{Na}$) $^+$, found: 284.9377 (Figure S20: ^1H and ^{13}C NMR of Methyl 2-iodobenzoate).

Methyl 4-iodobenzoate (**21**) [23]: White solid; mp 113–116 °C; ^1H NMR (400 MHz, CDCl_3): δ = 7.78 (d, J = 8.0 Hz, 2H), 7.72 (d, J = 8.0 Hz, 2H), 3.90 (s, 3H); ^{13}C NMR (100 MHz, CDCl_3): δ = 166.46, 137.69, 131.02, 129.57, 100.80, 52.30; HRMS (ESI-TOF) m/z : calcd for $\text{C}_8\text{H}_7\text{INaO}^{2+}$: 284.9386 ($\text{M} + \text{Na}$) $^+$, found: 284.9378 (Figure S21: ^1H and ^{13}C NMR of Methyl 4-iodobenzoate).

Methyl 3-iodobenzoate (**22**) [23]: White solid; mp 112–115 °C; ^1H NMR (400 MHz, CDCl_3): δ = 8.36 (m, 1H), 7.87 (d, J = 7.8 Hz, 1H), 7.85 (d, J = 7.8 Hz, 1H), 7.17 (t, J = 8.0 Hz, 1H), 3.91 (s, 1H); ^{13}C NMR (100 MHz, CDCl_3): δ = 165.51, 141.72, 138.44, 131.98, 130.06, 128.73, 93.87, 52.42; HRMS (ESI-TOF) m/z : calcd for $\text{C}_8\text{H}_7\text{INaO}^{2+}$: 284.9381 ($\text{M} + \text{Na}$) $^+$, found: 284.9371 (Figure S22: ^1H and ^{13}C NMR of Methyl 3-iodobenzoate).

Methyl 3-trifluoromethylbenzoate (**23**) [21,23]: Clear liquid; ^1H NMR (400 MHz, CDCl_3): δ = 8.28 (s, 1H), 8.18 (d, J = 8.0 Hz, 1H), 7.77 (d, J = 8.0 Hz, 1H), 7.53 (t, J = 8.0 Hz, 1H), 3.94 (s, 3H); ^{13}C NMR (100 MHz, CDCl_3): δ = 165.26, 132.50, 131.21 (q, $J_{\text{C-F}}$ = 31 Hz), 130.87, 130.55 (q, $J_{\text{C-F}}$ = 3.8 Hz), 129.07, 128.78 (q, $J_{\text{C-F}}$ = 4.0 Hz), 122.22 (q, $J_{\text{C-F}}$ = 270.5 Hz), 51.90; ^{19}F NMR (376 MHz, CDCl_3): δ = 63.41; HRMS (ESI-TOF) m/z : calcd for $\text{C}_9\text{H}_7\text{F}_3\text{NaO}^{2+}$: 227.0291 ($\text{M} + \text{Na}$) $^+$, found: 227.0286 (Figure S23: ^1H , ^{13}C and ^{19}F NMR of Methyl 3-trifluoromethylbenzoate).

Methyl 4-trifluoromethylbenzoate (**24**) [21,23]: Clear liquid; ^1H NMR (400 MHz, CDCl_3): δ = 8.11 (d, J = 8.0 Hz, 2H), 7.67 (d, J = 8.0 Hz, 2H), 3.94 (s, 3H); ^{13}C NMR (100 MHz, CDCl_3): δ = 165.51, 134.33 (q, $J_{\text{C-F}}$ = 32.5 Hz), 133.27, 129.76, 125.18 (q, $J_{\text{C-F}}$ = 4.0 Hz), 124.92 (q, $J_{\text{C-F}}$ = 272.5 Hz), 52.07; ^{19}F NMR (376 MHz, CDCl_3): δ = 63.60; HRMS (ESITOF) m/z : calcd for $\text{C}_9\text{H}_7\text{F}_3\text{NaO}^{2+}$: 227.0291 ($\text{M} + \text{Na}$) $^+$, found: 227.0294 (Figure S24: ^1H , ^{13}C and ^{19}F NMR of Methyl 4-trifluoromethylbenzoate).

Methyl 2-trifluoromethylbenzoate (**25**) [22,23]: Clear liquid; ^1H NMR (400 MHz, CDCl_3): δ = 7.78 – 7.71 (m, 2H), 7.59 – 7.57 (m, 2H), 3.92 (s, 3H); ^{13}C NMR (100 MHz, CDCl_3): δ = 167.11, 131.67, 131.10, 130.99, 128.70 (q, $J_{\text{C-F}}$ = 31.3 Hz), 126.59 (q, $J_{\text{C-F}}$ = 5.3 Hz), 126.43, 124.74, 52.51; ^{19}F NMR (376 MHz, CDCl_3): δ = 59.87; HRMS (ESI-TOF) m/z : calcd for $\text{C}_9\text{H}_7\text{F}_3\text{NaO}^{2+}$: 227.0292 ($\text{M} + \text{Na}$) $^+$, found: 227.0284 (Figure S25: ^1H , ^{13}C and ^{19}F NMR of Methyl 2-trifluoromethylbenzoate).

Methyl 4-*tert*-butylbenzoate (**26**) [22,23]: Clear liquid; ^1H NMR(400 MHz, CDCl_3): $\delta = 7.98$ (d, $J = 8.1$ Hz, 2H), 7.42 (d, $J = 8.1$ Hz, 2H), 3.90 (s, 3H), 1.32 (s, 9H); ^{13}C NMR (100 MHz, CDCl_3) $\delta = 166.73, 156.26, 129.44, 127.42, 125.19, 51.63, 34.87, 30.97$; HRMS (ESI-TOF) m/z : calcd for $\text{C}_{12}\text{H}_{17}\text{O}_2$ 193.3 (M+H) $^+$, found: 193.1 (Figure S26: ^1H and ^{13}C NMR of Methyl 4-*tert*-butylbenzoate).

Methyl 4-cyanobenzoate (**27**) [22]: White solid; mp 58–61 °C; ^1H NMR (400 MHz, CDCl_3): $\delta = 8.34$ – 8.26 (m, 2H), 7.84 (dt, $J = 8.0, 1.0$ Hz, 1H), 7.60 (dt, $J = 8.0, 1.2$ Hz, 1H), 3.97 (s, 3H); ^{13}C NMR (100 MHz, CDCl_3): $\delta = 165.04, 135.97, 133.63, 133.21, 131.39, 129.47, 117.85, 112.91, 52.69$; HRMS (ESITOF) m/z : calcd for $\text{C}_9\text{H}_7\text{NNaO}^{2+}$: 184.0366 (M + Na) $^+$, found: 184.0368 (Figure S27: ^1H and ^{13}C NMR of Methyl 4-cyanobenzoate).

o-Dimethyl phthalate (**28**) [23]: Clear liquid; ^1H NMR (400 MHz, CDCl_3): $\delta = 7.69$ (dd, $J = 6.5, 4.0$ Hz, 2H), 7.50 (dd, $J = 6.5, 4.0$ Hz, 2H), 3.88 (s, 6H); ^{13}C NMR (100 MHz, CDCl_3): $\delta = 167.70, 131.80, 130.97, 128.64, 52.29$; HRMS (ESI-TOF) m/z : calcd for $\text{C}_{10}\text{H}_{10}\text{NaO}^{4+}$: 217.0472 (M + Na) $^+$, found: 217.0476 (Figure S28: ^1H and ^{13}C NMR of *o*-Dimethyl phthalate).

p-Dimethyl terephthalate (**29**) [23]: White solid; mp 141–143 °C; ^1H NMR (400 MHz, CDCl_3): $\delta = 8.09$ (s, 4H), 3.94 (s, 6H); ^{13}C NMR (100 MHz, CDCl_3): $\delta = 166.09, 133.81, 129.44, 52.30$; HRMS (ESI-TOF) m/z : calcd for $\text{C}_{10}\text{H}_{10}\text{NaO}^{4+}$: 217.0472 (M + Na) $^+$, found: 217.0468 (Figure S29: ^1H and ^{13}C NMR of *p*-Dimethyl terephthalate).

m-Dimethyl terephthalate (**30**) [23]: White solid; mp 65–68 °C; ^1H NMR (400 MHz, CDCl_3): $\delta = 8.68$ (s, 1H), 8.21 (d, $J = 8.5$ Hz, 2H), 7.53 (t, $J = 8.5$ Hz, 1H), 3.95 (s, 6H); ^{13}C NMR (100 MHz, CDCl_3): $\delta = 166.04, 133.66, 130.58, 128.53, 52.23$; HRMS (ESI-TOF) m/z : calcd for $\text{C}_{10}\text{H}_{10}\text{NaO}^{4+}$: 217.0472 (M + Na) $^+$, found: 217.0488 (Figure S30: ^1H and ^{13}C NMR of *m*-Dimethyl terephthalate).

Methyl 3,4,5-trimethoxybenzoate (**31**) [22]: White solid; mp 81–83 °C; ^1H NMR (400 MHz, CDCl_3): $\delta = 7.30$ (s, 2H), 3.91 (s, 12H); ^{13}C NMR (100 MHz, CDCl_3): $\delta = 166.50, 152.82, 142.05, 125.04, 106.67, 60.72, 56.07, 52.05$; HRMS (ESI-TOF) m/z : calcd for $\text{C}_{11}\text{H}_{15}\text{O}_5$ 227.3 (M+H) $^+$, found: 227.1 (Figure S31: ^1H and ^{13}C NMR of Methyl 3,4,5-trimethoxybenzoate).

4. Conclusions

A series of iron-supported zirconium/titanium catalysts were synthesized for methyl benzoate synthesis. Catalyst composites with an iron/zirconium/titanium molar ratio of 2:1:1 demonstrated optimal catalytic effects on the synthesis of methyl benzoate compounds. A series of methyl benzoate compounds were synthesized using these catalysts to elucidate the catalytic mechanism. This catalyst effectively catalyzed the synthesis of various benzoic acids and methanol. The benzene ring of benzoic acid has a strong electron-withdrawing group ($-\text{NO}_2$, $-\text{CF}_3$) that can affect the ester yield. The catalyst can be easily separated from the reaction mixture after reaction completion and reused because it is a heterogeneous reaction system. Fe increased the catalyst activity owing to the increases in the catalyst surface and the number of acid sites.

Supplementary Materials: The following supporting information can be downloaded at <https://www.mdpi.com/article/10.3390/catal13060971/s1>, Figure S1: ^1H and ^{13}C NMR of Methyl benzoate; Figure S2: ^1H and ^{13}C NMR of Methyl 2-Methylbenzoate; Figure S3: ^1H and ^{13}C NMR of Methyl 3-Methylbenzoate; Figure S4: ^1H and ^{13}C NMR of Methyl 4-methylbenzoate; Figure S5: ^1H and ^{13}C NMR of Methyl 2-chlorobenzoate; Figure S6: ^1H and ^{13}C NMR of Methyl 3-chlorobenzoate; Figure S7: ^1H and ^{13}C NMR of Methyl 4-chlorobenzoate; Figure S8: ^1H and ^{13}C NMR of Methyl 3-bromobenzoate; Figure S9: ^1H and ^{13}C NMR of Methyl 4-bromobenzoate; Figure S10: ^1H and ^{13}C NMR of Methyl 2-bromobenzoate; Figure S11: ^1H , ^{13}C and ^{19}F NMR of Methyl 4-fluorobenzoate; Figure S12: ^1H , ^{13}C and ^{19}F NMR of Methyl 2-fluorobenzoate; Figure S13: ^1H , ^{13}C and ^{19}F NMR of Methyl 3-fluorobenzoate; Figure S14: ^1H and ^{13}C NMR of Methyl 4-nitrobenzoate; Figure S15: ^1H and ^{13}C NMR of Methyl 2-nitrobenzoate; Figure S16: ^1H and ^{13}C NMR of Methyl 3-nitrobenzoate; Figure S17: ^1H and ^{13}C NMR of Methyl 2-methoxybenzoate; Figure S18: ^1H and ^{13}C NMR of Methyl 3-methoxybenzoate; Figure S19: ^1H and ^{13}C NMR of Methyl 4-methoxybenzoate; Figure S20: ^1H and ^{13}C NMR of Methyl 2-iodobenzoate; Figure S21: ^1H and ^{13}C NMR of Methyl 4-iodobenzoate; Figure S22: ^1H and ^{13}C NMR of Methyl 3-iodobenzoate; Figure S23: ^1H , ^{13}C and ^{19}F NMR of Methyl

3-trifluoromethylbenzoate; Figure S24: ^1H , ^{13}C and ^{19}F NMR of Methyl 4-trifluoromethylbenzoate; Figure S25: ^1H , ^{13}C and ^{19}F NMR of Methyl 2-trifluoromethylbenzoate; Figure S26: ^1H and ^{13}C NMR of Methyl 4-tert-butylbenzoate; Figure S27: ^1H and ^{13}C NMR of Methyl 4-cyanobenzoate; Figure S28: ^1H and ^{13}C NMR of *o*-Dimethyl phthalate; Figure S29: ^1H and ^{13}C NMR of *p*-Dimethyl terephthalate; Figure S30: ^1H and ^{13}C NMR of *m*-Dimethyl terephthalate; Figure S31: ^1H and ^{13}C NMR of Methyl 3,4,5-trimethoxybenzoate.

Author Contributions: Conceptualization, writing—original draft preparation, X.Y. and C.S.; methodology, W.W. and H.W.; formal analysis, A.Z. and S.L.; writing—review and editing, X.Y. All authors have read and agreed to the published version of the manuscript.

Funding: This research was funded by the Natural Science Foundation of Bengbu University (2022ZR02zd), the Natural Science Project of Colleges and Universities in Anhui Province (KJ2020ZD65, KJ2021A1123, 2022AH051920), and the Provincial University Student Innovation and Entrepreneurship Project (s202211305007, s202211305005).

Data Availability Statement: No new data were created or analyzed in this study. Data sharing is not applicable to this article.

Conflicts of Interest: The authors declare no conflict of interest.

References

1. Zhao, Y.; Wang, Q.-F.; Song, B.-J.; Sun, P.-Y.; Zhang, S.-H.; Yao, Z.-L. The structure and hydrogenation performance for methyl benzoate of MnOx/ZrO₂-Cr₂O₃ catalyst. *J. Fuel Chem. Technol.* **2021**, *49*, 1709–1715. [[CrossRef](#)]
2. Yu, Z.; Dong, H.; Xie, X.; Liu, J.; Su, W. Continuous-Flow Diazotization for Efficient Synthesis of Methyl 2-(Chlorosulfonyl)benzoate: An Example of Inhibiting Parallel Side Reactions. *Org. Process Res. Dev.* **2016**, *20*, 2116–2123. [[CrossRef](#)]
3. Brossard, D.; Retailleau, P.; Dumontet, V.; Breton, P.; Desrat, S.; Roussi, F. Fast & easy preparation of 3D scaffolds from methyl benzoate by a diversity oriented synthesis strategy based on Diels–Alder and ene-reactions. *Org. Biomol. Chem.* **2017**, *15*, 5585–5592. [[PubMed](#)]
4. McDonald, C.E.; Nice, L.E.; Shaw, A.W.; Nestor, N.B. Calcium hypochlorite-mediated oxidation of primary alcohols to methyl esters. *Tetrahedron Lett.* **1993**, *34*, 2741–2744. [[CrossRef](#)]
5. Zhang, L.-R.; Liu, Z.-J.; Zhang, H.; Sun, J.; Luo, Y.; Zhao, T.-T.; Gong, H.-B.; Zhu, H.-L. Synthesis, biological evaluation and molecular docking studies of novel 2-(1,3,4-oxadiazol-2-ylthio)-1-phenylethanone derivatives. *Bioorganic Med. Chem.* **2012**, *20*, 3615–3621. [[CrossRef](#)]
6. Meira, C.S.; dos Santos Filho, J.M.; Sousa, C.C.; Anjos, P.S.; Cerqueira, J.V.; Dias Neto, H.A.; da Silveira, R.G.; Russo, H.M.; Wolfender, J.-L.; Queiroz, E.F.; et al. Structural design, synthesis and substituent effect of hydrazone-*N*-acylhydrazones reveal potent immunomodulatory agents. *Bioorganic Med. Chem.* **2018**, *26*, 1971–1985. [[CrossRef](#)]
7. Greulich, T.W.; Daniliuc, C.G.; Studer, A. N-Aminopyridinium Salts as Precursors for N-Centered Radicals—Direct Amidation of Arenes and Heteroarenes. *Org. Lett.* **2015**, *17*, 254–257. [[CrossRef](#)]
8. Venkateswarlu, V.; Aravinda Kumar, K.A.; Gupta, S.; Singh, D.; Vishwakarma, R.A.; Sawant, S.D. DMSO/I₂ mediated C–C bond cleavage of α -ketoaldehydes followed by C–O bond formation: A metal-free approach for one-pot esterification. *Org. Biomol. Chem.* **2015**, *13*, 7973–7978. [[CrossRef](#)]
9. Gao, Y.; Li, T.Y.; Zheng, W.J.; Zhou, Z.M.; Chen, L.X. Comprehensive spectral analysis of reaction of three aldehydes with ammonium sulfate and glycine. *Atmos. Environ.* **2022**, *291*, 14. [[CrossRef](#)]
10. Hosseini-Sarvari, M.; Sodagar, E. Esterification of free fatty acids (Biodiesel) using nano sulfated-titania as catalyst in solvent-free conditions. *Comptes Rendus Chim.* **2013**, *16*, 229–238. [[CrossRef](#)]
11. Hu, S.-L.; Zeng, Y.-J.; Wu, D.-Z.; Lou, W.-Y. A novel magnetic carbon-based solid acid catalyst suitable for efficient hydrolysis of cellulose. *Biomass Convers. Biorefinery* **2023**, *13*, 2207–2215. [[CrossRef](#)]
12. Ratthiwal, J.; Lazaro, N.; Reyes, A.A.R.; Osman, S.M.; Reubroycharoen, P.; Luque, R. Batch and continuous-flow room temperature furfural acetalization with ethanol over aluminophosphate (APAl) catalysts for biofuels production. *Fuel* **2023**, *332*, 126049. [[CrossRef](#)]
13. Smyrnioti, M.; Ioannides, T. Dimethyl Ether Hydrolysis over WO₃/ γ -Al₂O₃ Supported Catalysts. *Catalysts* **2022**, *12*, 396. [[CrossRef](#)]
14. Zhao, W.; Li, Z.; Wang, Y.; Fan, R.; Zhang, C.; Wang, Y.; Guo, X.; Wang, R.; Zhang, S. Ce and Zr Modified WO₃-TiO₂ Catalysts for Selective Catalytic Reduction of NO_x by NH₃. *Catalysts* **2018**, *8*, 375. [[CrossRef](#)]
15. Tomar, S.; Gangwar, S.; Kondamudi, K.; Upadhyayula, S. SO₃ decomposition over beta-SiC and SiO₂ supported CuFe₂O₄: A stability and kinetic study. *Int. J. Hydrog. Energy* **2020**, *45*, 21287–21296. [[CrossRef](#)]
16. Rasaki, S.A.; Zhang, B.X.; Anbalgam, K.; Thomas, T.; Yang, M.H. Synthesis and application of nano-structured metal nitrides and carbides: A review. *Prog. Solid State Chem.* **2018**, *50*, 1–15. [[CrossRef](#)]

17. Naik, A.P.; Mittal, H.; Wadi, V.S.; Sane, L.; Raj, A.; Alhassan, S.M.; Al Alili, A.; Bhosale, S.V.; Morajkar, P.P. Super porous TiO₂ photocatalyst: Tailoring the agglomerate porosity into robust structural mesoporosity with enhanced surface area for efficient remediation of azo dye polluted waste water. *J. Environ. Manag.* **2020**, *258*, 110029. [[CrossRef](#)]
18. Li, F.; Jiao, Y.; Liu, J.; Li, Q.; Guo, C.; Tian, C.; Jiang, B. Promoting the spatial charge separation by building porous ZrO₂@TiO₂ heterostructure toward photocatalytic hydrogen evolution. *J. Colloid Interface Sci.* **2020**, *561*, 568–575. [[CrossRef](#)]
19. Manikandan, N.; Lakshmi, B.; Shivakumara, S. Electrochemical capacitance performance of high surface area, porous hematite (α -Fe₂O₃) nanorods. *J. Mater. Sci. Mater. Electron.* **2022**, *33*, 7109–7118. [[CrossRef](#)]
20. Lv, C.P.; Du, D.; Wang, C.; Qin, Y.Y.; Ge, J.L.; Han, Y.S.; Zhu, J.J.; Liu, M.X. The Flower-like Co₃O₄ Hierarchical Microspheres for Methane Catalytic Oxidation. *Inorganics* **2022**, *10*, 49. [[CrossRef](#)]
21. Cao, Y.-F.; Li, L.-J.; Liu, M.; Xu, H.; Dai, H.-X. Palladium-Catalyzed, Copper(I)-Promoted Methoxycarbonylation of Arylboronic Acids with *O*-Methyl *S*-Aryl Thiocarbonates. *J. Org. Chem.* **2020**, *85*, 4475–4481. [[CrossRef](#)] [[PubMed](#)]
22. Zhu, Y.; Yan, H.; Lu, L.; Liu, D.; Rong, G.; Mao, J. Copper-Catalyzed Methyl Esterification Reactions via C–C Bond Cleavage. *J. Org. Chem.* **2013**, *78*, 9898–9905. [[CrossRef](#)] [[PubMed](#)]
23. Jiang, Y.; Pan, S.; Zhang, Y.; Yu, J.; Liu, H. Copper-Catalyzed Decarboxylative Methylation of Aromatic Carboxylic Acids with PhI(OAc)₂. *Eur. J. Org. Chem.* **2014**, *2014*, 2027–2031. [[CrossRef](#)]

Disclaimer/Publisher’s Note: The statements, opinions and data contained in all publications are solely those of the individual author(s) and contributor(s) and not of MDPI and/or the editor(s). MDPI and/or the editor(s) disclaim responsibility for any injury to people or property resulting from any ideas, methods, instructions or products referred to in the content.